Velocity-tunable cold Cs atomic beam from a magneto-optical trap

Xueshu Yan (颜学术)[1,2,4], Chenfei Wu (吴晨菲)[3,4], Jiaqiang Huang (黄家强)[3,4], Jianwei Zhang (张建伟)[1,2,4], and Lijun Wang (王力军)[1,2,3,4,*]

[1]*Department of Precision Instruments, Tsinghua University, Beijing 100084, China*
[2]*State Key Laboratory of Precision Measurement Technology and Instruments, Tsinghua University, Beijing 100084, China*
[3]*Department of Physics, Tsinghua University, Beijing 100084, China*
[4]*Joint Institute for Measurement Science (JMI), Tsinghua University, Beijing 100084, China*
**Corresponding author: lwan@tsinghua.edu.cn*

Received October 18, 2016; accepted December 23, 2016; posted online February 14, 2017

The construction of a two-dimensional magneto–optical trap with hollow cooling and pushing (2D-HP MOT) is reported in detail, and a velocity-tunable cold atomic beam produced by this 2D-HP MOT is demonstrated. The magneto–optical trap system, which is constructed by a transparent quartz tube, is low in price, easy to fabricate and assemble, and convenient for atomic trapping and detection. The mean axial velocity of the cold atomic beam can be tuned from 4.5 to 8 m/s, while the atomic flux remains at a level of 10^{10} atoms/s. This cold atomic beam source can be applied in the areas of high-precision measurements based on cold atoms.

OCIS codes: 020.3320, 020.7010, 300.2530.
doi: 10.3788/COL201715.040202.

Cold atomic beams are widely applied in various fields, such as atom interferometry[1–3], atomic frequency standards[4–6], atom optics[7], and cold atom physics[8], owing to their high atomic flux with low mean velocity, narrow velocity distribution, and small divergence. The cold atomic beam is generally produced by use of a vapor magneto-optical trap (MOT) source. The MOT source can be implemented in various configurations, such as a low-velocity intense source[9], a pure two-dimensional (2D) MOT[10], a two-dimensional plus ($2D^+$) MOT[11,12], and a 2D-HP MOT (H stands for the hollow cooling beam and P the thin pushing beam)[13].

An intense source of cold cesium atoms based on a 2D-HP MOT is demonstrated[13], with independent axial cooling and pushing. A pair of intense hollow laser beams is applied to accomplish the axial molasses cooling, and a weak and narrow Gaussian laser beam is used for the cold-atomic-beam pushing. The principle of the 2D-HP MOT and the dependence of the atomic flux on the pushing laser parameters have been investigated in detail in our previous work[13].

In this Letter, we report the construction of the 2D-HP MOT in detail and demonstrate a velocity-tunable intense cold atomic beam generated by this 2D-HP MOT. The vacuum chamber, which is constructed by a transparent quartz tube, is easy to fabricate and to install and is low cost. It is also convenient to observe the atomic cloud from all directions. The velocity-tunable property of the cold atomic beam is very useful for the applications of atom interferometry[2], atomic clocks[5,14,15], cold atomic collision[16], and ultra-high-vacuum MOT loading[17,18]. We also demonstrated that the mean axial velocity of the cold cesium beam can be tuned from 4.5 to 8.0 m/s, while its flux remains above 10^{10} atoms/s. Compared to some other similar works[10,12,19,20], the mean velocity of the intense cold atomic beam from the 2D-HP MOT is significantly slower, which can offer a longer interrogation time in the application of atomic beam clocks and larger Sagnac area in atomic interferometers. While some previous works also demonstrated similar cold beams with low axial velocities[21,22], the atomic flux obtained by the 2D-HP MOT is much more intense.

The scheme of the 2D-HP MOT is shown in Fig. 1(a). The lasers used for cooling and trapping are generated by two distributed-feedback laser diodes. The cooling laser is

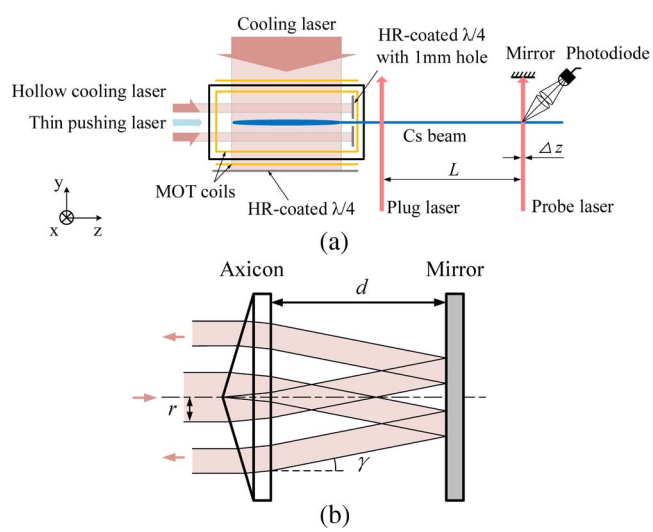

Fig. 1. (a) Scheme of the 2D-HP MOT. (b) Generation scheme of the collimating hollow beam by use of an axicon.

red-detuned from the $F = 4 \rightarrow F' = 5$ transition at -2.5Γ, where $\Gamma = 5.2$ MHz is the natural linewidth of the cesium D_2 line. The repumping laser to prevent the cesium atoms accumulating on energy level $F = 3$ is resonant with the $F = 3 \rightarrow F' = 4$ transition. In the radial direction, the laser beams contain cooling and repumping lasers, and they are circularly polarized. Two $\lambda/4$ wave plates with a high reflectance (HR) coating on one side and dimensions of 50 mm × 25 mm are installed in the X and Y directions to retro-reflect the cooling laser with reverse circular polarization. The sizes of radial laser beams are expanded to 40 mm × 20 mm with cylindrical lenses.

Two pairs of 140 mm × 100 mm rectangular coils separated symmetrically by 110 mm are installed in the X and Y directions to generate the gradient magnetic field for the MOT. The magnetic field gradient is set to 10 G/cm. Along the Z direction, it retains no magnetic field gradient.

In the longitudinal direction, one intense hollow laser beam, retro-reflected by a 25-mm HR-coated $\lambda/4$ wave plate, is applied for Doppler cooling. At the center of the wave plate, one 1-mm hole is drilled for outcoupling the cold atomic beam. The hollow beam is derived from the cooling laser and generated by use of an axicon, shown in Fig. 1(b). The radial intensity distribution has a relationship with the refraction angle γ of the axicon and the interval d between the axicon and the mirror. When the radius of the incident beam is r, the internal and external radii of the hollow beam will be $(2d \cdot \tan\gamma - r)$ and $2d \cdot \tan\gamma$, respectively.

The generation of the cold atomic beam in the 2D-HP MOT is independently controlled by the pushing laser beam. The pushing beam is a thin, collimated Gaussian beam, and its frequency is tuned by an acousto-optic modulator and power adjusted by an attenuator. The pushing beam is concentric with the hollow beam but spatially separated. Under the radiation of the pushing laser beam, the cold atoms will accelerate forward to leave the MOT. The acceleration of the cold atoms can be written as

$$\dot{v}_z(t) = \frac{\hbar k \Gamma}{2m} \frac{s}{1 + s + 4(\delta - k \cdot v_z(t))^2/\Gamma^2}, \tag{1}$$

where k is the wave vector, Γ is the natural linewidth, $\delta = W_L - W_a$ is the pushing laser detuning, $s = I/I_s$ is the saturation coefficient, m is the cesium atom mass, and $v_z(t)$ is the axial velocity. Thus, the axial velocity of the cold atoms coming out of the MOT varies with the power and detuning of the pushing laser.

The axial velocity distribution is analyzed by use of a time-of-flight method. By detecting the time dependence of the decreasing fluorescence signal $u(\tau)$ after blocking the cold atomic beam, the axial velocity distribution $\rho(v)$ can be obtained as

$$\rho(v) = -\frac{1}{k_c} \frac{t}{\Delta z} \frac{\mathrm{d}u(\tau)}{\mathrm{d}\tau}, \qquad \text{with } v = \frac{L}{\tau}, \tag{2}$$

where k_c is the calibration coefficient of the detection system, $\Delta z = 1$ mm is the width of the detection zone, and $L = 300$ mm is the travel distance of the cold atoms before the detection zone. The total flux of the atomic beam Φ is an integral of the velocity distribution,

$$\Phi = \int_0^\infty \rho(v) \mathrm{d}v. \tag{3}$$

The three-dimensional view of the transparent MOT system is given in Fig. 2(a). The main part of the system is the quartz-tube vacuum chamber. The internal diameter of the tube is 55 mm. The MOT device placed inside is a quadrupole titanium holder, which keeps a BK7 glass plate and a $\lambda/4$ wave plate perpendicular to the tube axis. This $\lambda/4$ wave plate is HR coated, and we drilled a 1-mm hole at the center. Cold atoms are cooled and trapped within the region between the two plates. The connection between the quartz tube and the metal flange is sealed by rubber O-rings. The section view of the sealing arrangement is shown in Fig. 2(b). Three pressure rings and two rubber O-rings are assembled on the quartz tube in proper order. A bolt fastening locks the holddown and the flange. Additionally, a Teflon washer is placed at the end of the tube to protect the quartz tube from the axial stress. With high mounting forces, the rubber O-ring fills the groove between the two pressure rings and

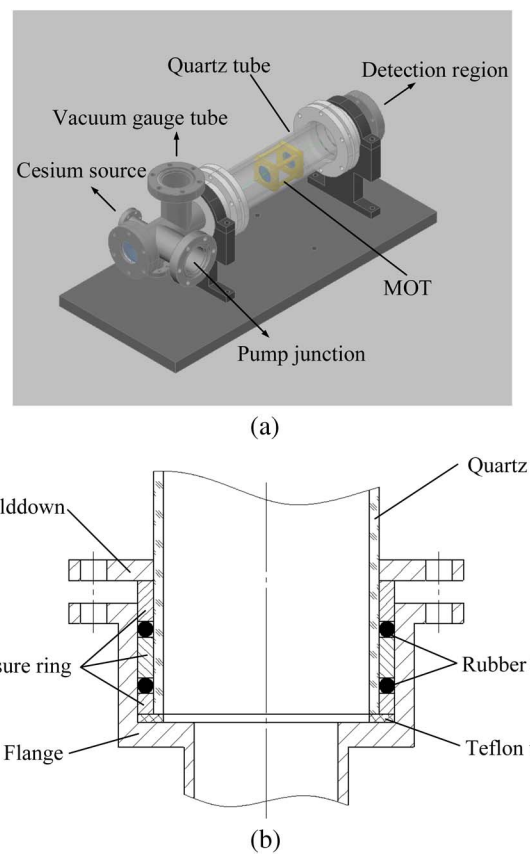

Fig. 2. (a) Three-dimensional view of the transparent MOT system. (b) Section view of the vacuum sealing arrangement.

accommodates the imperfections of the surface. This sealing arrangement can maintain the vacuum at the level of 10^{-6} Pa, limited by the outgassing of the O-rings. In the experiment, the vacuum of the MOT is maintained at about 1.2×10^{-5} Pa, which is consistent with the design expectations and is good enough for most of the cold-atom experiments.

As shown in Fig. 2(a), one end of the tube is connected to a cesium reservoir, a vacuum gauge, and a turbo pump, and the other end is connected to the detection region. The cesium reservoir is heated to about 35°C to produce a dense enough cesium vapor. In the detection region, an ion pump is additionally used to get a higher vacuum at 3.5×10^{-6} Pa.

One of the main advantages of this MOT system is that the transparency of the quartz tube is greatly convenience for the optical setup and provides a full view angle for outside observers like CCD cameras. Additionally, compared to a classical metallic cavity and a vacuum window with a conflat flange, no subassemblies of this MOT system require complicated mechanical process. This makes the MOT system simple to fabricate and low cost. Moreover, the quartz-tube vacuum chamber is beneficial to realize a lightweight and miniaturized system.

A CCD camera is applied to observe the cold atoms in real time. According to the working principle of the 2D-HP MOT, the axial cooling and pushing are accomplished by two separated laser beams. Thus, the dependence of the fluorescence of the cold atoms on the laser beams in the MOT is demonstrated. In Fig. 3, the fluorescence pictures of cold atoms in four different axial-laser conditions are shown, where the four conditions are no axial laser beams, only pushing beam, only hollow beam, and hollow beam and pushing beam. With the hollow cooling beam off, it is hard to see a cold atomic cloud within the MOT, no matter whether the pushing beam is on or off [see Figs. 3(a) and 3(b)]. This reveals that the pushing beam makes no contribution to the axial cooling. When only the hollow beam is on, it is obvious that a thick cold atomic cloud is captured, as shown in Fig. 3(c). When the pushing beam and the hollow cooling beam are both on, as shown in Fig. 3(d), the fluorescence signal of atomic cloud is less than the one in Fig. 3(c) due to the fact that part of the cold atoms is pushed out to generate the atomic beam. This shows the hollow cooling and the pushing beams work as designed.

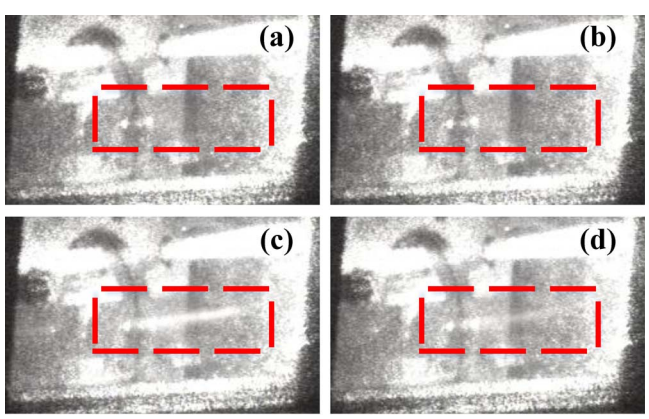

Fig. 3. Fluorescence pictures of cold atoms in the MOT at four axial-laser conditions. (a) No axial laser beams. (b) Pushing beam only. (c) Hollow beam only. (d) Hollow beam and pushing beam.

By the unbalance radiation pressure induced by the pushing beam, part of the cold cesium atoms is accelerated and pushed out of the MOT. According to Eq. (1), we have

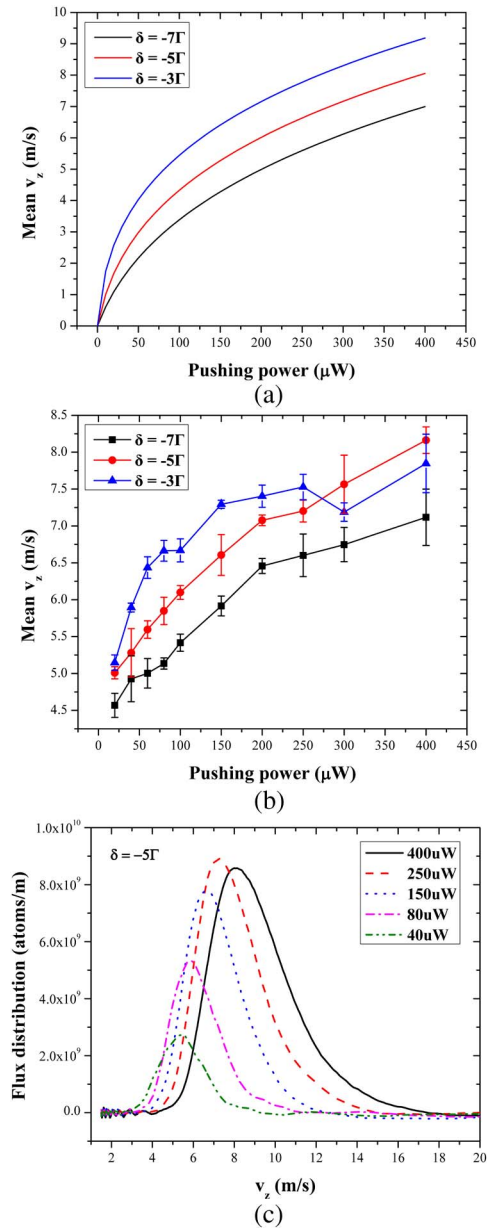

Fig. 4. Tunable axial velocity of the cold cesium beam. (a) Calculated atomic beam velocity as a function of the pushing power with different detunings. (b) Experimental data showing the variation of the mean axial velocity v_z with the power of -7Γ (black square), -5Γ (red circle), and -3Γ-detuned (blue triangle) pushing beam. (c) Experimental data showing the variation of the axial velocity distributions with the power of a -5Γ-detuned pushing beam.

simulated the mean velocity based on a simplified model as below. We consider only the longitudinal motion of the cesium atoms and the effect of the pushing laser and assume that the initial velocity is ignorable after cooling. The calculated atomic beam velocity as a function of the pushing power is illustrated in Fig. 4(a).

In the experiment, while the pushing beam is red-detuned, the mean axial velocity of the cold atomic beam can be varied with the pushing power from 4.5 to 8.0 m/s. Meanwhile, the atomic flux is maintained at the level of 10^{10} atoms/s. The variations of the mean axial velocity that depend on the power of the pushing laser are shown in Fig. 4(b), where the detunings are -7Γ, -5Γ, and -3Γ. These experimental results are mostly in agreement with the theoretical simulation, except for the data of -3Γ, with the power over 300 μW. We have done the measurements repeatedly but still failed to explain this phenomenon well. In the range of low pushing powers, there is some deviation between the experiment and the simulation. As a result of gravity, very low-velocity atoms are lost before they reach the detection region. Therefore, the measured mean velocity is faster than the actual mean velocity. We believe this is the main reason for the deviation between the experiment and the simulation. The variation of the axial velocity distribution with the power of a -5Γ-detuned pushing beam is shown in Fig. 4(c). When the pushing power is 40 μW, the mean axial velocity is 5.2 m/s. As the power increases, the mean velocity gradually increases to a maximum. When the pushing power is 400 μW, the mean velocity reaches 8.1 m/s. The atomic flux increases quickly with the increase of the pushing laser power. It can reach 4×10^{10} atoms/s when the pushing power is 400 μW.

Generally, the 2D-HP MOT can generate a rather intense cold cesium beam in a wide range of velocities by regulating the power of a red-detuned pushing beam. This cold atomic beam can be used to develop a continuous atom clock.

In conclusion, we demonstrate the generation of velocity-tunable intense cold cesium atomic beams by a transparent MOT configuration of the 2D-HP MOT. Owing to the application of the quartz tube, the 2D-HP MOT in this Letter is simple to fabricate, easy to install, and rather inexpensive. Meanwhile, the transparent vacuum wall of the MOT provides great convenience for experiments, for example, in optical setups and for external observations. By setting the pushing beam to be red-detuned and regulating the pushing power, the 2D-HP MOT can generate a rather intense cold cesium beam with a mean velocity ranging from 4.5 to 8.0 m/s. This property makes it very convenient to carry out experiments and optimize the experimental parameters for our future work on a continuous cold cesium atomic clock.

This work was supported by the National Natural Science Foundation of China under Grant No. 11304177. The authors especially acknowledge Yanying Feng and Chi Xu for the helpful discussions.

References

1. D. W. Keith, C. R. Ekstrom, Q. A. Turchette, and D. E. Pritchard, Phys. Rev. Lett. **66**, 2693 (1991).
2. H. Xue, Y. Feng, S. Chen, X. Wang, X. Yan, Z. Jiang, and Z. Zhou, J. Appl. Phys. **117**, 094901 (2015).
3. T. Müller, T. Wendrich, M. Gilowski, C. Jentsch, E. M. Rasel, and W. Ertmer, Phys. Rev. A **76**, 063611 (2007).
4. J. Vanier, Appl. Phys. B **81**, 421 (2005).
5. P. Thomann, M. Plimmer, G. Di Domenico, N. Castagna, J. Guéna, G. Dudle, and F. Füzesi, Appl. Phys. B **84**, 659 (2006).
6. D. Lv, B. Wang, T. Li, and L. Liu, Chin. Opt. Lett. **8**, 735 (2010).
7. S. Zhou, J. Qian, S. Zhang, and Y. Wang, Chin. Opt. Lett. **14**, 070202 (2016).
8. M. H. Anderson, J. R. Ensher, M. R. Matthews, C. E. Wieman, and E. A. Cornell, Science **269**, 198 (1995).
9. Z. T. Lu, K. L. Corwin, M. J. Renn, M. H. Anderson, E. A. Cornell, and C. E. Wieman, Phys. Rev. Lett. **77**, 3331 (1996).
10. J. Schoser, A. Batär, R. Löw, V. Schweikhard, A. Grabowski, Y. B. Ovchinnikov, and T. Pfau, Phys. Rev. A **66**, 023410 (2002).
11. K. Dieckmann, R. J. C. Spreeuw, M. Weidemüller, and J. T. M. Walraven, Phys. Rev. A **58**, 3891 (1998).
12. S. J. Park, J. Noh, and J. Mun, Optic. Comm. **285**, 3950 (2012).
13. J. Huang, X. Yan, C. Wu, J. Zhang, and L. Wang, Chin. Phys. B **25**, 63701 (2016).
14. H. Wang and G. Iyanu, in *2010 IEEE International Frequency Control Symposium* (2010), p. 454.
15. A. Jallageas, L. Devenoges, M. Petersen, J. Morel, L. Bernier, P. Thomann, and T. Südmeyer, J. Phys. Conf. **723**, 012010 (2016).
16. J. Weiner, V. S. Bagnato, S. Zilio, and P. S. Julienne, Rev. Mod. Phys. **71**, 1 (1999).
17. E. Donley, T. Heavner, and S. Jefferts, IEEE Trans. Instrum. Meas. **54**, 1905 (2005).
18. F. Sorrentino, Y. Lien, G. Rosi, L. Cacciapuoti, M. Prevedelli, and G. Tino, New J. Phys. **12**, 095009 (2010).
19. S. Chaudhuri, S. Roy, and C. S. Unnikrishnan, Phys. Rev. A **74**, 023406 (2006).
20. N. Castagna, J. Guéna, M. Plimmer, and P. Thomann, Eur. Phys. J. Appl. Phys. **34**, 21 (2006).
21. S. Weyers, E. Aucouturier, C. Valentin, and N. Dimarcq, Opt. Commun. **143**, 30 (1997).
22. H. Wang and W. F. Buell, J. Opt. Soc. Am. B **20**, 2025 (2003).